Volume 54
Number 32
28 August 2025
Pages 12053-12406

Dalton Transactions

An international journal of inorganic chemistry

rsc.li/dalton

ISSN 1477-9226

PAPER

Valentin Bockmair *et al.*

Shrinking of C–S bonds of organosulfonic acids in superacidic media—investigation of the protonation of methanesulfonic acid and benzenesulfonic acid and their limits

ROYAL SOCIETY OF CHEMISTRY

Dalton Transactions

ROYAL SOCIETY OF CHEMISTRY

PAPER

View Article Online
View Journal | View Issue

Cite this: *Dalton Trans.*, 2025, **54**, 12169

Shrinking of C–S bonds of organosulfonic acids in superacidic media—investigation of the protonation of methanesulfonic acid and benzenesulfonic acid and their limits†

Valentin Bockmair, * Tong Xu, Dirk Hollenwäger and Andreas J. Kornath‡

Received 11th April 2025,
Accepted 21st July 2025

DOI: 10.1039/d5dt00864f

rsc.li/dalton

The reactions of methanesulfonic acid and benzenesulfonic acid in the binary superacidic systems HF/MF_5 (M = As and Sb) were investigated to explore the strengthening effects of protonation on the C–S bond and the limits of the protonability of sulfonic acids. Herein, we report the monoprotonated species of methanesulfonic acid and benzenesulfonic acid, respectively. The salts were characterized by low-temperature vibrational spectroscopy, single-crystal X-ray diffraction, and NMR spectroscopic measurements. The experimental data are discussed together with quantum chemical calculations at the B3LYP/aug-cc-pVTZ-level of theory.

Introduction

The organosulfonic acids methanesulfonic acid (MSA) and benzenesulfonic acid (BSA) represent the smallest alkyl- and the smallest benzylic sulfonic acids. Methanesulfonic acid and benzenesulfonic acid have various pharmaceutical and catalytic applications. The salts of methanesulfonic acid are used for the treatment of Parkinson's disease.[1] Besides the use as detergents, salts of benzenesulfonic acid known as besilates (INN) or besylates (USAN) are widespread in many pharmaceuticals, *e.g.*, amlodipine besylate for the treatment of high blood pressure and chronic stable angina pectoris. Besylates can stabilize the active ingredient amlodipine and improve its solubility so that the drug can be more easily resorbed in the body.[2]

Benzenesulfonic acid serves as a catalyst in chemical reactions (*e.g.* in resin synthesis)[3] and as an intermediate in the production of resorcinol and phenol. MSA is also used as a catalyst in many syntheses, for example in cyclisation[4] and polymerisation reactions.[5] Furthermore, MSA is used as an electrolyte and exhibits strong self-dissociation (autoprotolysis), as depicted in Scheme 1.

The high electrolyte conductivity enables lower consumption in electrochemical processes, particularly for Sn/Pb solder electroplating. Additionally, MSA is considered environmentally friendly as it is biodegradable and is used for the replacement of other electrolytes[6]

Marked by strong self-dissociation, similar to sulfuric acid or hydrogen fluoride,[7,8] methanesulfonic acid ($pK_a = -0.6$) and benzenesulfonic acid ($pK_a = 0.7$) are strong acids compared to common organic acids.[9,10] Compared with other sulfonic acids, however, MSA and BSA are rather less acidic, and therefore find no applications in superacid chemistry.

Recent studies about the protonation of sulfonic acids in binary superacidic systems HF/MF_5 (M = As and Sb) have only achieved the isolation of monoprotonated species, yet (see Scheme 2).[11–13]

These investigations were based on acidity to determine which compound undergoes protonation.[11,13] As these studies were based on highly acidic compounds, sulfonic acid moieties were attached to electron-withdrawing groups, such as triflic acid or fluorosulfonic acid, instead of electron-rich sub-

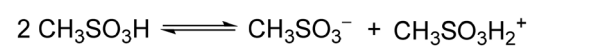

Scheme 1 Self-dissociation of MSA.

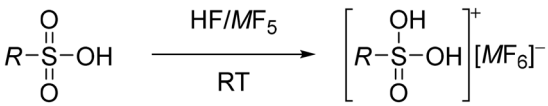

Scheme 2 General protonation reaction of sulfonic acids in superacidic media (R = F_3C, $EtNH_3$, and F and M = As and Sb).

Department Chemie Ludwig-Maximilians-Universität München, Butenandtstr. 5–13, 81377 München, Germany. E-mail: Valentin.Bockmair@cup.uni-muenchen.de

†Electronic supplementary information (ESI) available. CCDC 2419553–2419556 and 2422284. For ESI and crystallographic data in CIF or other electronic format see DOI: https://doi.org/10.1039/d5dt00864f

‡Prof. Dr A. J. Kornath passed away unexpectedly in March 2024.

stituents. MSA and BSA contain an electron-rich backbone and are therefore highly stable against desulfonation and resistant towards hydrolysis. Therefore, we expected that the protonation of the sulfonyl group would be easily achieved and a hemi- or monoprotonated species might be accessed in the rather weak binary superacidic system HF/BF_3.[14]

Furthermore, molecules with a stabilizing substituent effect, *i.e.* a positive inductive effect of R could possibly achieve a higher degree of protonation of the sulfonium moiety. This is of particular interest as no diprotonation of the sulfonyl moieties has been achieved yet (Scheme 3).

In order to explore the protonation chemistry of the sulfonyl compounds RSO_2OH (R = CH_3 and Ph) the conversions in the binary superacidic systems HF/L (L = BF_3, AsF_5, and SbF_5) were investigated. The aim of this work was to figure out the influence on the C–S bond and whether hemi- ($[(RSO_3H)_2H]^+$), monoprotonated (sulfonium ions $[RSO_3H_2]^+$), or even diprotonated species (disulfonium ions $[RSO_3H_3]^{2+}$) can be isolated.

Results and discussion

Synthesis of protonated MSA, $[MeSO_3H_2][AsF_6]$ (2) and $[MeSO_3H_2][Sb_2F_{11}]$ (3)

Methanesulfonic acid was reacted in the binary superacidic systems HF/BF_3 and HF/MF_5 (M = As and Sb) at room temperature. Therefore, an excess of solvent (HF) and at least two equivalents of Lewis acid (BF_3 or MF_5) were added to achieve full protonation of the sulfonic acid moiety if possible. Unreacted Lewis acid and solvent were removed under dynamic vacuum at −78 °C.

No conversion of MSA in the binary superacidic system HF/BF_3 was observed. Instead of protonation of MSA (**1**) according to Scheme 4, the starting material only recrystallized from solution as identified by single-crystal X-ray diffraction.

Conversion of MSA in the binary superacidic systems HF/MF_5 (M = As and Sb) resulted in the isolation of the monoprotonated species (**2**) and (**3**). According to Scheme 5, the products (**2**) and (**3**) were obtained in the form of colorless solids. The protonated species were further characterized by NMR and low-temperature vibrational spectroscopy, as well as single-crystal X-ray diffraction.

The monoprotonated species of methanesulfonic acid were stable when tested up to room temperature.

Synthesis of protonated BSA, $[PhSO_3H_2][AsF_6]$ (4) and $[PhSO_3H_2][Sb_2F_{11}]$ (5)

Benzenesulfonic acid was reacted in the binary superacidic systems HF/BF_3 and HF/MF_5 (M = As and Sb) at room temperature. Therefore, an excess of solvent (HF) and at least two equivalents of Lewis acid (BF_3 or MF_5) were added to achieve full protonation of the sulfonic acid moiety if possible. Unreacted Lewis acid and solvent were removed under dynamic vacuum at −78 °C. According to Scheme 6, no conversion of BSA in the binary superacidic system HF/BF_3 was observed as only a brown amorphous residue of the starting material was obtained.

Conversion of BSA in the binary superacidic system HF/MF_5 (M = As, Sb) yielded the isolation of the monoprotonated species (**4**) and (**5**), according to Scheme 7. The protonated species were further characterized by NMR and low-temperature vibrational spectroscopy. Single crystals of (**5**) were investigated by X-ray diffraction.

The monoprotonated species of benzenesulfonic acid were stable when tested up to room temperature. As the hexafluoroarsenate salt (**4**) was only poorly soluble in anhydrous hydrogen fluoride, attempts to recrystallize the salt in thionyl fluoride were made. Single crystal measurements of the product indicated the formation of the corresponding sulfonyl fluoride

Scheme 3 The protonation of sulfonic acids RSO_3H, (R = CH_3 and Ph and L = BF_3, AsF_5, and SbF_5).

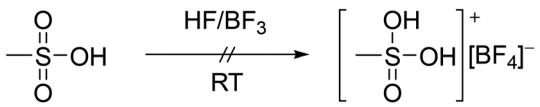

Scheme 4 Expected protonation of $MeSO_3H$ in the binary superacidic system HF/BF_3.

Scheme 5 The protonation of $MeSO_3H$ in binary superacidic media (M = As (**2**) and Sb (**3**)).

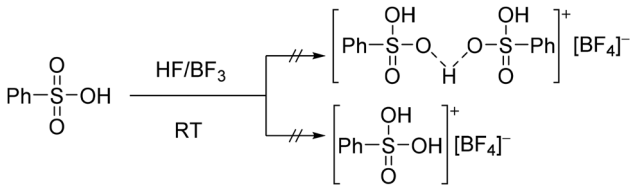

Scheme 6 Expected hemi- or monoprotonation of $PhSO_3H$ in the binary superacidic system HF/BF_3.

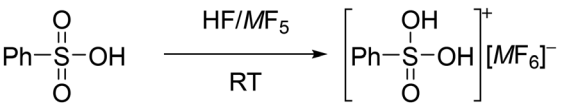

Scheme 7 The protonation of $PhSO_3H$ in binary superacidic media (M = As (**4**) and Sb (**5**)).

instead of the desired product (see ESI section 2.5;† see Scheme 8).

Crystal structures

MSA (1). For better comparison, the structure was redetermined at low temperature. As already reported by Wickleder *et al.*,[15] MSA (**1**) crystallizes in the monoclinic space group $P2_1/c$ with four formula units per unit cell as depicted in Fig. 1.

Selected geometric data are listed in Table 1, showing the S–O single bond (1.548(1) Å), as well as two S═O double bonds (1.445(2) and 1.429(2) Å) within the 3σ area as reported in general literature[16] and for other organosulfonic acids.[14,17]

The C–S bond length of 1.743(3) Å is consistent with those of other sulfonic acid compounds[17] or sulfonic acid anhydrides[15] and can be considered as slightly shortened with respect to comparison values.[16] Thereby, it strongly differs from trifluoromethanesulfonic acid[18] and its protonated species,[11] where the C–S bond length is found to be elongated.

In its packing, methanesulfonic acid is stabilized by two medium-strong hydrogen bonds, forming an infinitive chain and building up an antiparallel layered structure. Weaker donor–acceptor interactions (C(H)···O) can be localized in the layers (C(H1B)···O2), as well as in the connecting link of two molecules in the antiparallel layers (C(H1C)···O3i) with each other.

The asymmetric unit of **1** and short contacts are illustrated in Fig. 2.

$[MeSO_3H_2][AsF_6]$ (2). The arsenic hexafluoride salt of monoprotonated methanesulfonic acid (**2**) crystallizes in the triclinic space group $P\bar{1}$ with two formula units per unit cell as depicted in Fig. 3.

In the structure of $[MeSO_3H_2][AsF_6]$, the bond length of S1–O2 (1.519(2) Å) is significantly elongated compared to that of MSA (**1**) (1.445(2) Å) and is in the range of a formal S–O single bond (1.432 Å)[16] indicating successful protonation. In contrast, the S═O (1.409(2) Å) and C–S (1.729(3) Å) bond lengths are significantly shortened through the shift of electron density towards O2, by protonation.

In its packing, protonated methanesulfonic acid is surrounded by five $[AsF_6]^-$ anions and four $[MeSO_3H_2]^+$ cations (Fig. 4). Two strong hydrogen bonds are formed with $[AsF_6]^-$ anions O2(H3)···F1i (2.549(2) Å), O1(H2)···F5 (2.562(3) Å), as well as one medium-strong hydrogen bond O1(H2)···F3 (2.885(3) Å). The C···F contact, C1···F2i (3.118(4) Å), and three weaker donor–acceptor interactions are built up on the methyl group C1(H1B)···F6 (3.206(4) Å), C1(H1C)···O3 (3.266(3) Å), and C1(H1A)···F4 (3.378(4) Å). Furthermore, $[MeSO_3H_2][AsF_6]$ is stabilized by orbital interactions in the packing $n_{O1} \rightarrow \sigma^*_{O1i}$, $n_{O1i} \rightarrow \sigma^*_{O1}$, which can be detected at a distance of 2.872(3) Å, as well as $n_{O2} \rightarrow \sigma^*_{O2i}$, $n_{O2i} \rightarrow \sigma^*_{O2}$ 2.761(3) Å, respectively (Table 2).

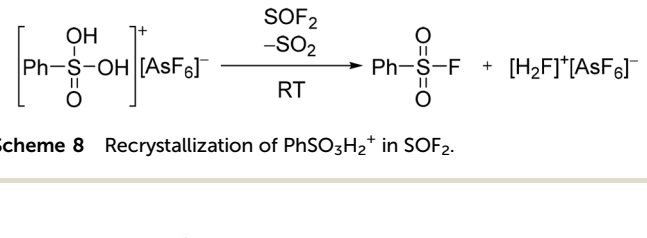

Scheme 8 Recrystallization of $PhSO_3H_2^+$ in SOF_2.

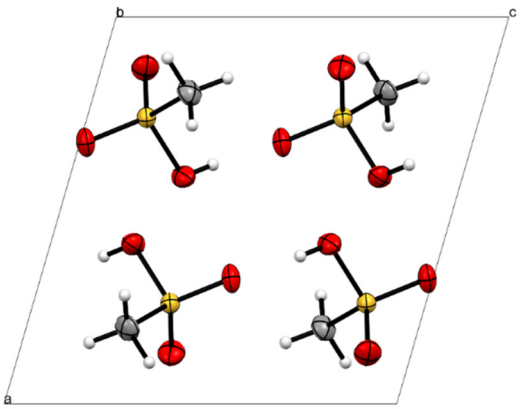

Fig. 1 Crystal structure of MSA (**1**), viewed along the *b* axis (displacement ellipsoids with 50% probability).

Table 1 Selected bond lengths [Å] and angles [°] of MSA (**1**) and donor–acceptor distances

Bond lengths [Å]			
S1–O1	1.548(1)	S1–O3	1.429(2)
S1–O2	1.445(2)	S1–C1	1.743(3)
Bond angles [°]			
O1–S1–C1	104.5(1)	O2–S1–O1	104.95(9)
O1–S1–O3	110.53(9)	O2–S1–O3	117.27(9)
Dihedral angles [°]			
O1–S1–C1–H1C	−174(2)	O3–S1–C1–H1B	−177(2)
O2–S1–C1–H1B	179(2)		
Interatomic distances [Å]			
O1(H2)···O2ii	2.619(2)	O3···(H1Ci)C1i	3.527(3)
C1(H1B)···O2ii	3.283(3)	C1(H1C)···O3i	3.527(3)

Symmetry codes: i = $-x$, $-y$, $-z$; ii = x, $1/2 - y$, $1/2 + z$.

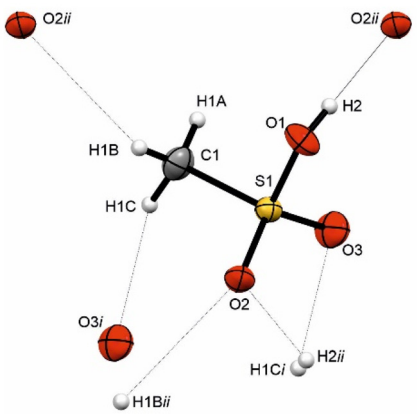

Fig. 2 Short contacts of the asymmetric unit of **1** (displacement ellipsoids with 50% probability). Symmetry codes: i = $-x$, $-y$, $-z$; ii = x, $1/2 - y$, $1/2 + z$.

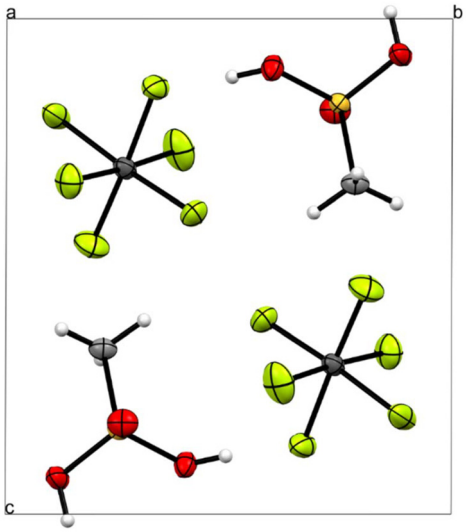

Fig. 3 Crystal structure of $[MeSO_3H_2][AsF_6]$ (**2**), viewed along the *a* axis (displacement ellipsoids with 50% probability).

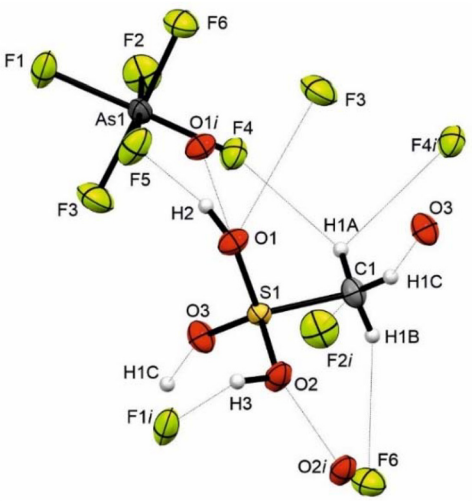

Fig. 4 Short contacts of the asymmetric unit of **2** (displacement ellipsoids with 50% probability). Symmetry codes: i = −*x*, −*y*, −*z*.

Table 2 Selected bond lengths [Å] and angles [°] of $[MeSO_3H_2][AsF_6]$ (**2**) and donor–acceptor distances

Bond lengths [Å]			
S1–O1	1.521(2)	S1–O3	1.409(2)
S1–O2	1.519(2)	S1–C1	1.729(3)
Bond angles [°]			
O1–S1–C1	107.8(1)	O2–S1–O1	102.1(1)
O1–S1–O3	113.2(1)	O2–S1–O3	115.5(1)
Dihedral angles [°]			
O1–S1–C1–H1C	53(2)	O3–S1–C1–H1B	−59(3)
O2–S1–C1–H1B	67(3)	O3–S1–C1–H1C	180(2)
Interatomic distances [Å]			
O2(H3)···F1i	2.549(2)	C1···F2i	3.118(4)
O1(H2)···F5	2.562(3)	C1(H1B)···F6	3.206(4)
O2···O2i	2.761(3)	C1(H1C)···O3	3.266(3)
O1···O1i	2.872(3)	C1(H1A)···F4	3.378(4)
O1(H2)···F3	2.885(3)		

Symmetry codes: i = −*x*, −*y*, −*z*.

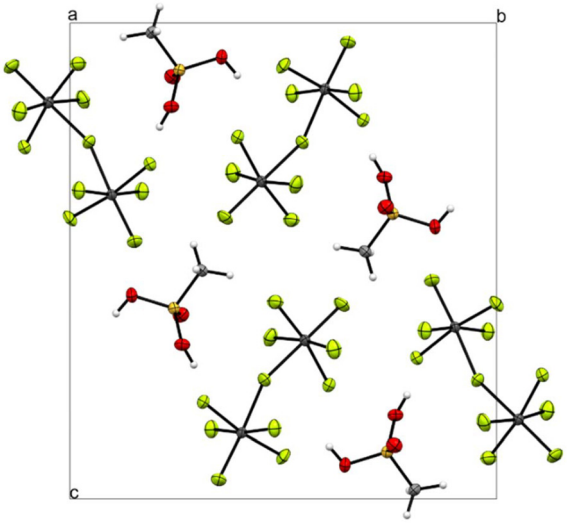

Fig. 5 Crystal structure of $[MeSO_3H_2][Sb_2F_{11}]$ (**3**), viewed along the *a* axis (displacement ellipsoids with 50% probability).

$[MeSO_3H_2][Sb_2F_{11}]$ (3). The undecafluoridodiantimonate(v) salt of monoprotonated methanesulfonic acid (**3**) crystallizes in the monoclinic space group $P2_1/c$ with four formula units per unit cell as depicted in Fig. 5.

In the structure of $[MeSO_3H_2][Sb_2F_{11}]$, the S–O bond lengths are similar to those of the $[AsF_6]^-$ salt and show an elongation of S1–O2 (1.525(5) Å). The S=O double bond is significantly shortened, shrinking up to 1.404(5) Å, as well as the C–S bond shrinking up to 1.726(6) Å, respectively.

The $[MeSO_3H_2]^+$ cation in the packing is surrounded by six $[Sb_2F_{11}]^-$ anions and two other cations, arranged as zigzag chains along the *a* axis (Fig. 6).

In contrast to the less bulky $[AsF_6]^-$ anion, the $[Sb_2F_{11}]^-$ salt forms many hydrogen bonds (seven) in the range of 2.591(5)–2.999(6) Å and weaker donor–acceptor interactions (six) instead of forming C···F or orbital interactions at a distance of 3.184(8)–3.472(8) Å (Table 3).

$[PhSO_3H_2][Sb_2F_{11}]$ (5). The undecafluoridodiantimonate(v) salt of monoprotonated benzenesulfonic acid (**5**) crystallizes in the monoclinic space group $P2_1$ with two formula units per unit cell as depicted in Fig. 7.

In contrast to the crystal structure of BSA,[17] there are no crystallographically independent cations within the structure (Fig. 8).

In the structure of $[PhSO_3H_2][Sb_2F_{11}]$, the S–O single bond lengths differ significantly in accordance with the strength of the attached hydrogen bonds as the steric requirement of the phenyl ring does not allow two closer contacts. Therefore, the bonds S1–O1 (1.523(4) Å) and S1–O2 (1.496(4) Å) differ by

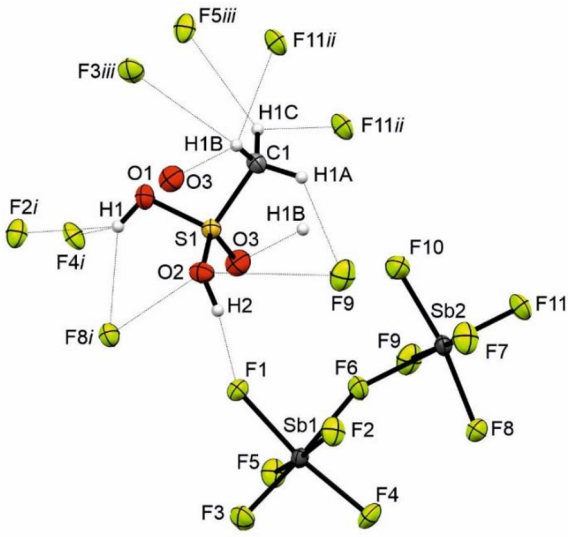

Fig. 6 Short contacts of the asymmetric unit of **3** (displacement ellipsoids with 50% probability). Symmetry codes: i = $-x$, 1/2 + y, 1/2 − z; ii = $-x$, $-y$, $-z$; iii = x, 1/2 − y, 1/2 + z.

Table 3 Selected bond lengths [Å] and angles [°] of $[MeSO_3H_2][Sb_2F_{11}]$ (**3**) and donor–acceptor distances

Bond lengths [Å]			
S1–O1	1.525(5)	S1–O3	1.404(5)
S1–O2	1.526(5)	S1–C1	1.726(6)
Bond angles [°]			
O1–S1–C1	100.7(3)	O2–S1–O1	105.5(3)
O1–S1–O3	115.2(3)	O2–S1–O3	113.5(3)
Dihedral angles [°]			
O1–S1–C1–H1C	−60.0	O3–S1–C1–H1B	−175.2
O2–S1–C1–H1B	−49.4		
Interatomic distances [Å]			
O2(H2)···F1	2.591(5)	O2(H2)···F5	3.211(7)
O1(H1)···F2i	2.720(6)	C1(H1A)···F9	3.235(8)
O2(H2)···F8i	2.913(5)	C1(H1B)···F11ii	3.253(7)
O1(H1)···F8i	2.930(6)	C1(H1C)···F5iii	3.327(7)
O2(H2)···F9	2.975(6)	C1(H1B)···F3iii	3.367(7)
O1(H1)···F4i	2.999(6)	C1(H1B)···O3	3.472(8)
C1(H1C)···F11ii	3.184(8)		

Symmetry codes: i = $-x$, 1/2 + y, 1/2 − z; ii = $-x$, $-y$, $-z$; iii = x, 1/2 − y, 1/2 + z.

length. The S=O double bond (1.398(5) Å) is significantly shortened compared to those of the starting material (1.420 (1)–1.441(1) Å), and appears to be even shorter than in the methanesulfonium ion (1.404(5) and 1.409(2) Å). In addition, the C–S bond length 1.717(5) Å is significantly shortened compared to those of BSA (1.749(1) Å and 1.760(1) Å) (Table 4).

Vibrational spectroscopy

The low-temperature Raman spectra of MSA (**1**) and its protonated species $[MeSO_3H_2][AsF_6]$ (**2**) and $[MeSO_3H_2][Sb_2F_{11}]$ (**3**) are illustrated in Fig. 9. In Table 5, selected observed Raman and IR frequencies of **2** and **3** are listed together with the quantum chemically calculated frequencies of the $[MeSO_3H_2]^+$·HF cation as well as their assignments. The low-temperature Raman spectra and IR spectra of BSA and its protonated species $[MeSO_3H_2][AsF_6]$ (**4**)/$[MeSO_3H_2][Sb_2F_{11}]$ (**5**) are illustrated in Fig. 10.

Raman and IR frequencies of **4** and **5** are listed together with the quantum chemically calculated frequencies of the $[PhSO_3H_2]^+$·HF cation as well as their assignments.

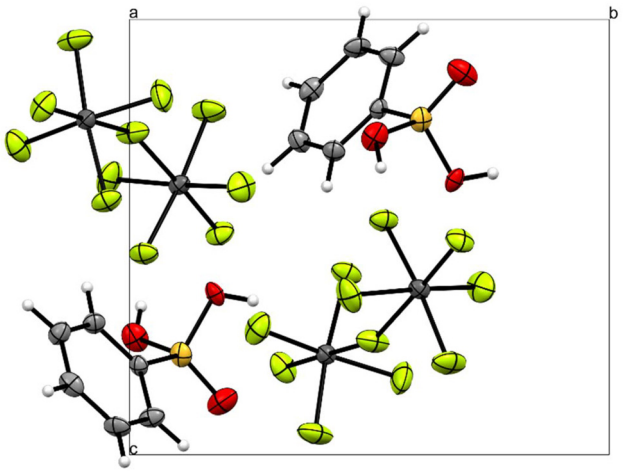

Fig. 7 Crystal structure of $[PhSO_3H_2][Sb_2F_{11}]$ (**5**), viewed along the *a* axis (displacement ellipsoids with 50% probability).

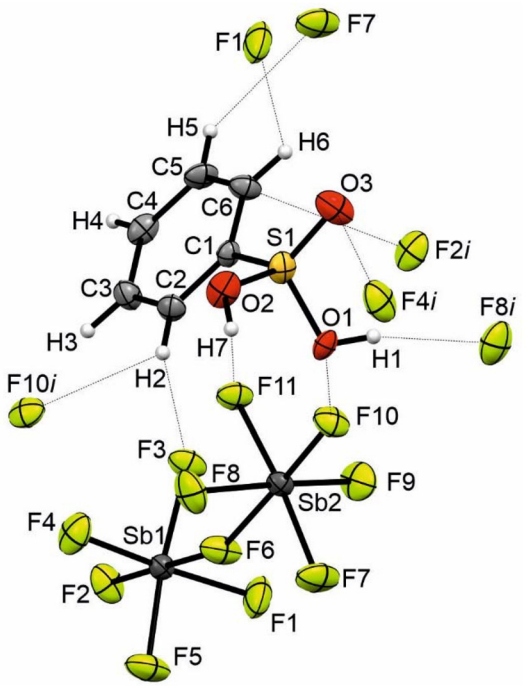

Fig. 8 Short contacts of the asymmetric unit of **5** (displacement ellipsoids with 50% probability). Symmetry codes: i = $-x$, 1/2 + y, $-z$.

Table 4 Selected bond lengths [Å] and angles [°] of $[PhSO_3H_2][Sb_2F_{11}]$ (**5**) and donor–acceptor distances

Bond lengths [Å]			
S1–O1	1.523(4)	C2–C3	1.376(8)
S1–O2	1.496(4)	C3–C4	1.384(9)
S1–O3	1.398(5)	C4–C5	1.396(8)
S1–C1	1.717(5)	C5–C6	1.376(8)
C1–C2	1.384(8)	C6–C1	1.395(8)
Bond angles [°]			
O1–S1–C1	105.8(2)	O2–S1–O1	101.2(2)
O1–S1–O3	110.5(3)	O2–S1–O3	117.1(3)
Dihedral angles [°]			
O1–S1–C1–C6	−118.8(4)	O3–S1–C1–C2	−176.2(4)
O2–S1–C1–C6	134.5(4)		
Interatomic distances [Å]			
F11···(H7)O2	2.504(6)	C6(H6)···F1	3.187(7)
F8i···(H1)O1	2.924(5)	C2(H2)···F10i	3.255(7)
F10···O1	2.931(5)	C5(H5)···F7	3.279(7)
F4i···O3	2.975(6)	C2···F3	3.322(7)
C6···F2i	3.058(7)		

Symmetry codes: i = $-x$, $1/2 + y$, $-z$.

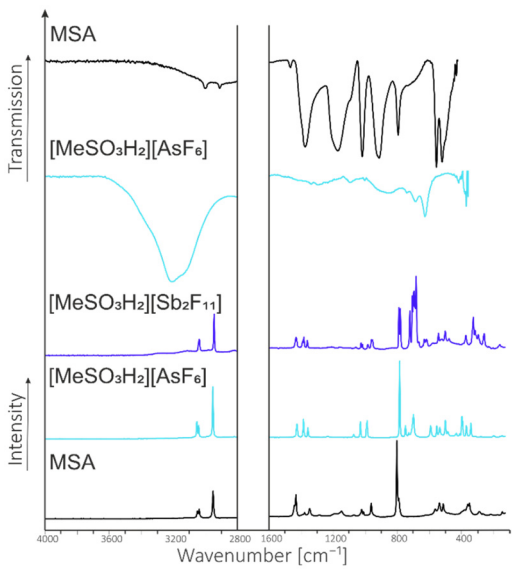

Fig. 9 Low-temperature IR and Raman spectra of MSA **1** and protonated species **2** and **3**.

Vibrational spectra of MSA (1) and monoprotonated species of MSA, $[MeSO_3H_2][AsF_6]$ (2)/$[MeSO_3H_2][Sb_2F_{11}]$ (3). The methanesulfonium cation ($[MeSO_3H_2]^+$) has C_1 symmetry with 24 expected fundamental vibrational modes (A), of which all are Raman- and IR-active. The complete analysis of the vibrational frequencies is provided in the ESI in Tables S18 and 19.† Selected observed vibrational frequencies and calculated frequencies are presented in Table 5.

The O–H stretching vibration is observed at 3218 cm^{-1} in the IR spectrum, blue-shifted from 3031 cm^{-1} compared with that of the starting material, visualizing the O-protonation. Due to poor polarizability, the O–H stretching vibration cannot be detected in the Raman spectra. Direct comparison of the expected O–H vibration frequencies with the calculated frequencies shows that the influence of hydrogen bonds in the structure concerning its vibrations is strong, as high deviations appear for pure gas phase calculations. The combined S=O stretching vibrations are in good accordance with the calculated values of 1309 and 910 cm^{-1}. The S=O stretching vibrations detected at 962 and 928 cm^{-1} (Ra) show a significant red shift from 1123 cm^{-1} (Ra), whereas the stretching vibrations detected at 1332 and 1334 cm^{-1} (Ra) stay nearly unaffected by the protonation. The expected S–O stretching vibration at 839 cm^{-1} was detected at 759 or 763 cm^{-1} (Ra), respectively, red-shifted from that of the starting material (901 cm^{-1} (Ra)). The C–S stretching vibrations observed at 673 or 694 cm^{-1} (Ra), respectively, are in good accordance with the calculated value of 682 cm^{-1}. The C–S stretching vibrations show high deviation from that of the starting material (534 cm^{-1} (Ra)), calculated to be at 661 cm^{-1} and detected at 669 cm^{-1} (Ra).

A significant shift of the vibrations can be seen compared to those of the starting material,[19] but due to the combination of vibrations, the variations are not consequently shifted as expected, analogous to O-protonation of other sulfur-based compounds.[20–22]

Vibrational spectra of BSA and the monoprotonated species of BSA, $[PhSO_3H_2][AsF_6]$ (4)/$[PhSO_3H_2][Sb_2F_{11}]$ (5). The benzosulfonium cation ($[PhSO_3H_2]^+$) has C_1 symmetry with 45 expected fundamental vibrational modes (A), of which all are Raman- and IR-active. The complete analysis of the vibrational frequencies is provided in the ESI in Tables S20 and 21.† Selected observed vibrational frequencies and calculated frequencies are presented in Table 6.

The O–H stretching vibrations are observed in the IR spectra at 3682 and 3115 cm^{-1} for the $[AsF_6]^-$ salt and at 3668 cm^{-1} and 3198 cm^{-1} for the $[Sb_2F_{11}]^-$ salt. Whereas the O–H stretching vibrations of the $[AsF_6]^-$ salt are red-shifted, the O–H stretching vibrations of the $[Sb_2F_{11}]^-$ salt remain nearly unaffected by the protonation. The S=O stretching vibrations detected at 1307 cm^{-1} (Ra) and 1290 cm^{-1} (IR) for the $[AsF_6]^-$ salt and at 1269 cm^{-1} (IR) for the $[Sb_2F_{11}]^-$ salt show significant deviations compared with those of the starting material. The S–O stretching vibrations observed at 908 cm^{-1}, 833 cm^{-1} (Ra) and 835 cm^{-1} (IR) for the $[AsF_6]^-$ salt and at 905 cm^{-1} and 847 cm^{-1} (IR) for the $[Sb_2F_{11}]^-$ salt show a similar significant blue shift for both salts compared with those of the starting material. The C–S stretching vibrations were detected to be slightly blue shifted in good accordance with the calculations, indicating the strengthening of the C–S bond upon protonation.

The vibrational spectroscopic analysis of BSA was challenging due to the high absorption of BSA and protonated species. Therefore, the products could only be poorly characterized by Raman spectroscopy. The observed and calculated vibrational frequencies differ partially as vibration coupling

Table 5 Selected observed vibrational frequencies [cm^{-1}] of MSA and $[MeSO_3H_2]^+$ salts (**2**) and (**3**) with calculated vibrational frequencies [cm^{-1}] of $[MeSO_3H_2]^+$

MSA[a] (Ra)	IR	$[MeSO_3H_2][AsF_6]$[a] (Ra)	IR	$[MeSO_3H_2][Sb_2F_{11}]$[a] (Ra)	$[MeSO_3H_2]^+$ [b,c]	Assignment
3031(17)	3031(w)		3218(vs,br)		3551(278/62)	ν(O–H)
		3055(22)			3082(1710/161)	ν(O–H)
		3043(17)		3039(21)	3058(16/41)	$\nu(CH_3)$
2945(80)	2944(w)	2954(67)		2947(52)	2958(37/125)	$\nu(CH_3)$
1304(6)	1256(w,sh)	1332(14)	1275(vw)	1334(19)	1309(153/6)	ν(S═O) + $\gamma(CH_3)$
1123(37)	1127(s)	962(23,sh)		928(20)	910(157/4)	ν(S═O) + $\tau(CH_2)$
901(10)	879(s)	759(100)	839(w,br)	763(61)	839(166/5)	$\tau(CH_3)$ + ν(S–O)
667(1)	671(w,sh)	673(31,sh)	687(m)	694(56)	682(29/17)	ν(C–S)
534(50)	530(vs)		615(w)	669(81)	661(71/5)	ν(C–S)

[a] Abbreviations for IR intensities: vs = very strong, s = strong, m = medium, w = weak, sh = shoulder, br = broad. Experimental Raman intensities are relative to a scale of 1 to 100. [b] Calculated at the B3LYP/aug-cc-pVTZ level of theory. Scaling factor: 0.968. [c] IR intensities in km mol^{-1}; Raman intensities in $Å^4$ u^{-1}.

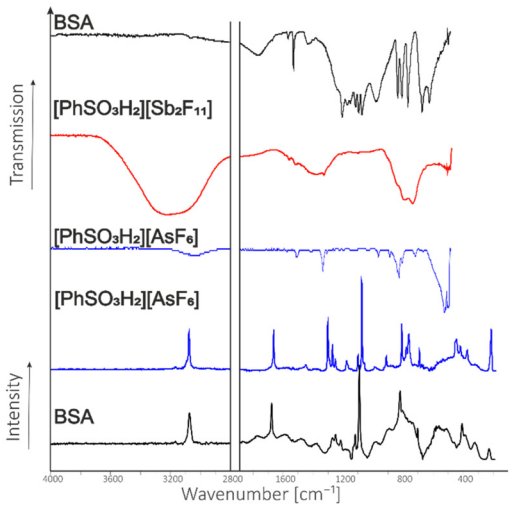

Fig. 10 Low-temperature Raman spectra of BSA and protonated species **4** and **5**.

occurs and the discussed salt differs by the formation of contacts. In general, the same trend of shifts can be found, as for the vibrations of MSA.

NMR spectroscopy

The ^1H and $^{13}C\{^1H\}$ NMR spectra of the starting materials MSA and BSA as well as pure MSA were measured at room temperature in $CDCl_3$. Protonated species were measured in anhydrous HF at room temperature with acetone-d^6 as the external reference. In order to screen that no side reaction takes place under the applied conditions ^{19}F spectra were recorded.

Selected observed NMR shifts in aHF are listed in Table 7. The complete NMR spectroscopic data and the measured NMR spectra are provided in the ESI (chapter 4).†

In the ^1H NMR spectrum of MSA in $CDCl_3$ two singlet signals of different intensities were detected for the sulfonic acid and the methyl moiety, which were assigned to the pure compound and the H_3O^+ species. This was verified by the exclusion of conformer variation by the measurement of the pure compound. Upon protonation, the sulfonium moiety ($SO_3H_2^+$) does not show a visible ^1H signal due to fast proton exchange and the methyl group is only weakly shielded by the shortening of the C–S bond. While the protons are shifted downfield, the methyl carbon is deshielded by 1.8 ppm. In the ^{19}F spectra of the protonated species of MSA the detected signals can be assigned to AsF_5 (−66.10 ppm) and $H[AsF_6]$

Table 6 Selected observed vibrational frequencies [cm^{-1}] of BSA and $[PhSO_3H_2]^+$ salts (**4**) and (**5**) with calculated vibrational frequencies [cm^{-1}] of $[PhSO_3H_2]^+$

BSA[a]	IR	$[PhSO_3H_2][AsF_6]$[a]	IR	$[PhSO_3H_2][Sb_2F_{11}]$ (IR)[a]	$[PhSO_3H_2]^+$ [b,c]	Assignment
	3660(vw)		3682(vw)	3668(vw)	3567(252/68)	ν(O–H)
	3173(vw)		3115(w)	3198(vs)	3145(1891/280)	ν(O–H)
3074(36)	3064(vw)	3076(43)			3112.52(4/202)	ν(ring)
		3028(3)	3036(w)		3108.20(3/100)	ν(ring)
		2935(2)			3096.89(1/83)	ν(ring)
1371(1)	1352(w)	1307(4)	1290(vw)	1269(m)	1305(73/6)	ν(S═O) + δ(ring)
1130(12)	1123(m)	1224(55)	1211(m)	1213(m)	1295(114/12)	ν(S═O) + δ(ring)
813(3)	753(s)	908(5)		905(vw)	904(232/7)	ν(S–O)
		833(16)	835(w)	847(vw)	821(210/18)	ν(S–O)
648(1)	685(vs)		696(s)	671(s)	690(14/14)	ν(C–S)
501(10)		533(4)	534(vw)	534(vw)	537(80/3)	ν(C–S)

[a] Abbreviations for IR intensities: vs = very strong, s = strong, m = medium, w = weak, sh = shoulder, br = broad. Experimental Raman intensities are relative to a scale of 1 to 100. [b] Calculated at the B3LYP/aug-cc-pVTZ level of theory. Scaling factor: 0.968. [c] IR intensities in km mol^{-1}; Raman intensities in $Å^4$ u^{-1}.

Table 7 ^{1}H-and ^{13}C-NMR data of MSA, BSA and its protonated species $[MeSO_3H_2][AsF_6]$ (2)/$[PhSO_3H_2][Sb_2F_{11}]$ (5) in [ppm]

	$[H_3O][MeSO_3]$	MSA	$[MeSO_3H_2][AsF_6]$ (2)	BSA	$[PhSO_3H_2][Sb_2F_{11}]$ (5)
^{1}H	11.99 (s,H_3O^+,3H) 4.47 (s,CH_3,3H)	11.11 (s,SO_3H,1H) 3.42 (s,CH_3,3H)	3.27 (s,CH_3,3H)	11.27 (s,SO_3H,1H) 7.82 (s_d,C_o,2H) 7.53 (s_t,C_p,1H) 7.42 (s_t,C_m,2H)	9.58 (s,$SO_3H_2^+$,2H) 7.60 (s_d,C_o,2H) 7.53 (s_t,C_p,1H) 7.26 (s_t,C_m,2H)
$^{13}C\{^{1}H\}$	39.25(CH_3)	39.30 (CH_3)	37.48 (CH_3)	138.23 (C_q) 133.41 (C_p) 129.22 (C_m) 126.73 (C_o)	141.24 (C_q) 131.09 (C_p) 129.26 (C_m) 127.59 (C_o)

Abbreviations for labelling of carbon atoms: q = quaternary, *p* = *para*, *m* = *meta*, *o* = *ortho*.

(−168.18 ppm), as well as to the decomposition product (54.64 ppm), which could not be identified further.

In the ^{1}H NMR spectrum of BSA in $CDCl_3$ a signal of the sulfonic acid (11.27 ppm) and three signals (7.82, 7.53 and 7.42 ppm) of the phenyl moiety were detected. The different signals of the phenyl ring show the expected splitting and intensities of the compound. The protonated sulfonium moiety was detected at 9.58 ppm in the ^{1}H spectrum. Similar to that for MSA, a weak ^{1}H shift (shielding effect) can be seen upon protonation of BSA (7.60 7.53 and 7.26 ppm), whereas the carbon atoms of the phenyl ring are shifted downfield up to 3 ppm (C_q). Surprisingly the ^{13}C signals of the carbon atoms in the *meta* position appear nearly unaffected from protonation. In the ^{19}F spectra of the protonated species of BSA two signals of the decomposition can be located at 57.14 and 38.71 ppm, as well as the $[Sb_2F_{11}]^-$ anion at −126.05 ppm.

Theoretical calculations

The structural optimization of MSA, BSA, $[MeSO_3H_2]^+$ and $[PhSO_3H_2]^+$ was carried out using DFT methods at the B3LYP/aug-cc-pVTZ-level of theory at 298 K. The monoprotonated species of BSA and MSA were calculated with solvated HF to simulate solid-state effects and intermolecular interactions. For MSA, the strongest hydrogen bonds were calculated with water molecules to simulate adequate gas phase basicity. For the calculation of BSA, pure gas phase calculations were performed.

The MEPs were calculated together with natural population analysis charges (NPAs) to gain insight into the charge distribution of the sulfonium acid moiety and the carbon in the α-position. In Fig. 11–14, the mapped electrostatic potentials (MEPs) of MSA, $[MeSO_3H_2]^+$, BSA, and $[PhSO_3H_2]^+$ are shown. The ESI† lists the NPA and NBO charges of the shown compounds.

In the MEP of MSA (see Fig. 11), the C–S bond is only weakly polarized as the negative electrostatic potential (red) is located at the oxygen atoms of the sulfonic acid moiety, and the positive electrostatic potential (blue) is located at the hydrogen atoms, particularly on the acidic proton of the sulfonic acid moiety.

In the MEP of protonated MSA (see Fig. 12), the negative electrostatic potential (red) is located at the remaining sulfuryl oxygen. The positive electrostatic potential (blue) can be located at the sulfur atom, as well as at the protons of the sulfonium moiety. Compared with the starting material, the carbon and sulfur are deshielded, as a π hole can be localized at the sulfur atom.

In the MEP of BSA (see Fig. 13), negative electrostatic potential (red) is located at the oxygen atoms of the sulfonic acid moiety and the positive electrostatic potential (blue) is located at the hydrogen atoms, particularly on the acidic proton of the sulfonic acid moiety.

In the MEP of protonated BSA (see Fig. 14), the negative electrostatic potential (red) is located at the remaining sulfuryl oxygen. The positive electrostatic potential is located at the protons (blue). The sulfur atom, as well as the quaternary C atom, is less deshielded due to delocalization on the π system as depicted by the NPA charges.

The NPA charges indicate that for the protonated species of MSA the methyl group shows only weak back-donation of electron density, whereas the protonated species BSA shows delocalisation of the positive charge along the C–S bond.

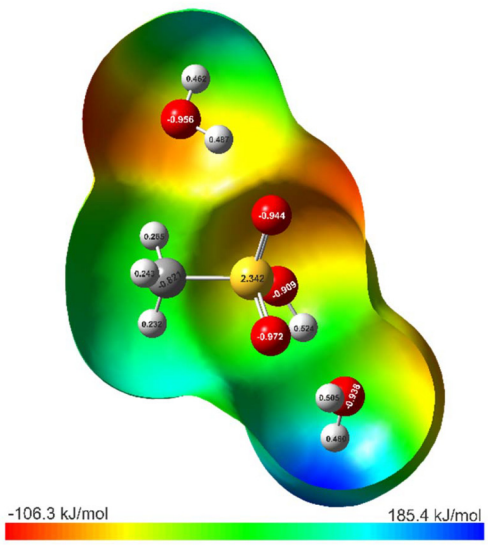

Fig. 11 Molecular 0.0004 bohr^{-3} 3D isosurfaces with MEP on a color scale ranging from −106.3 kJ mol^{-1} (red) to 185.4 kJ mol^{-1} (blue). The electrostatic potential isosurfaces and the NPA charges have been calculated for $MeSO_3H{\cdot}2H_2O$.

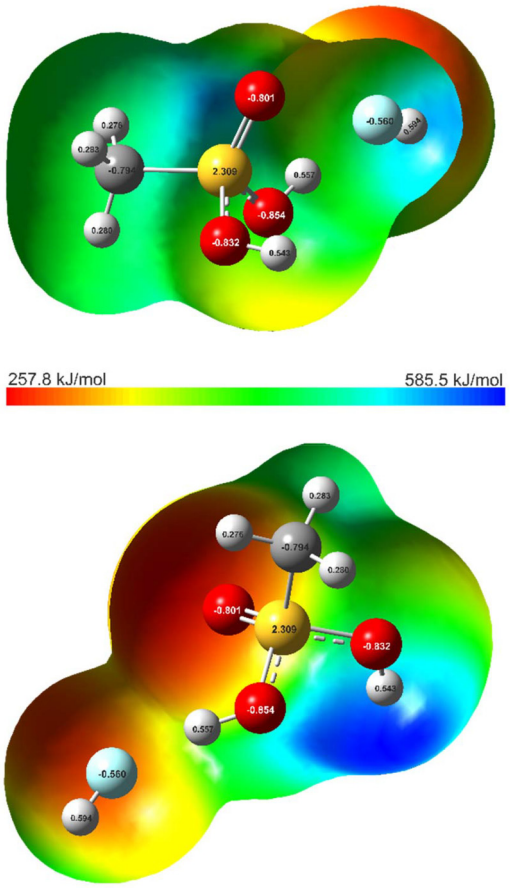

Fig. 12 Molecular 0.0004 bohr^{-3} 3D isosurfaces with MEP on a color scale ranging from 257.8 kJ mol^{-1} (red) to 585.5 kJ mol^{-1} (blue). The electrostatic potential isosurfaces and the NPA charges have been calculated for $[MeSO_3H_2]^+$·HF.

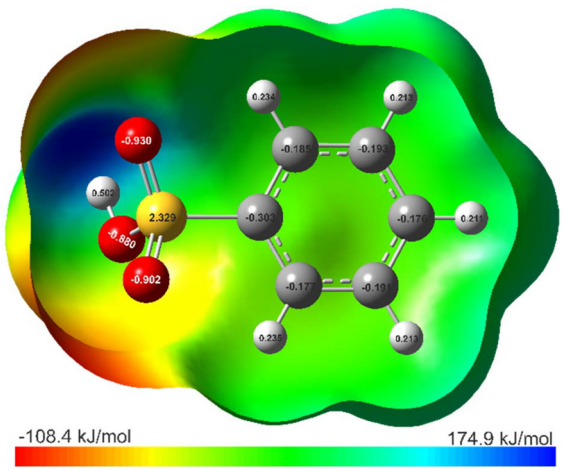

Fig. 13 Molecular 0.0004 bohr^{-3} 3D isosurfaces with MEP on a color scale ranging from –108.4 kJ mol^{-1} (red) to 174.9 kJ mol^{-1} (blue). The electrostatic potential isosurfaces and the NPA charges have been calculated for $PhSO_3H$.

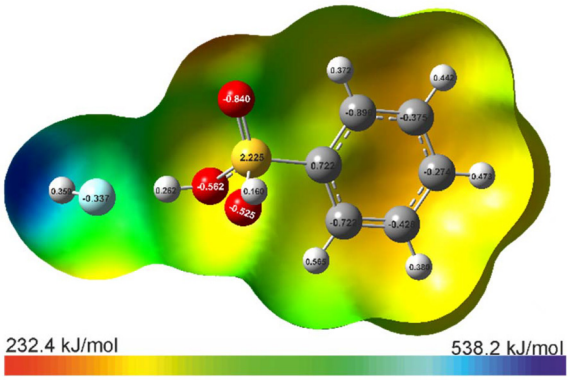

Fig. 14 Molecular 0.0004 bohr^{-3} 3D isosurfaces with MEP on a color scale ranging from 232.4 kJ mol^{-1} (red) to 538.2 kJ mol^{-1} (blue). The electrostatic potential isosurfaces and the NPA charges have been calculated for $[PhSO_3H_2]^+$·HF.

Table 8 Calculated bond lengths [Å] on the B3LYP/aug-cc-pVTZ level of theory in comparison with experimental values

	S═O	SO	SO	C–S
MSA	1.450	1.460	1.596	1.784
Exp.	1.429(2)	1.445(2)	1.548(1)	1.743(3)
$[MeSO_3H_2]^+$	1.423	1.567	1.559	1.773
Exp.	1.409(2)	1.519(2)	1.521(2)	1.729(3)
BSA	1.440	1.450	1.632	1.786
Exp.[17]	1.420(1)	1.439(1)	1.557(1)	1.749(1)
	1.424(1)	1.441(1)	1.553(1)	1.760(1)
$[PhSO_3H_2]^+$	1.431	1.551	1.591	1.745
Exp.	1.398(5)	1.496(4)	1.523(4)	1.717(5)

Red shortened and blue elongated according to the calculation of the starting material.

As observed in the single X-ray structures, protonation causes a significant shortening of the remaining S═O bond and C–S bond due to electron-withdrawing effects. Furthermore, elongation of the new S–O bonds was observed for experimental and calculated values as depicted in Table 8.

Experimental

General

Caution! The hydrolysis of BF_3, AsF_5, SbF_5 and the prepared salts (**2**, **3**, **4** and **5**) might form HF, which burns skin and causes irreparable damage. Safety precautions must be taken while using and handling these materials.

Apparatus and materials

The reactions were carried out according to Schlenk's standard procedure with a stainless-steel vacuum line. Fluorinated ethylene propylene (FEP)/per-fluoralkoxy (PFA) reactors sealed with a stainless-steel valve were used for all of the reactions in

superacid media. Both the vacuum line and the reactors were dried with fluorine before use. Raman spectroscopic studies at low temperatures were performed using a Bruker MultiRAM FT-Raman spectrometer with Nd:YAG laser excitation (λ = 1064 cm^{-1}) under vacuum at −196 °C. For measurement, the synthesized compounds were transferred into a cooled glass cell at low temperatures. IR spectra were recorded in a vacuum using a Bruker Vertex-80 VFTIR spectrometer. A small amount of the synthesized samples was placed on a CsBr single-crystal plate in a room-temperature cell for measurement.[23] Low-temperature single-crystal X-ray diffraction of MSA (**1**), $[MeSO_3H_2][AsF_6]$ (**2**), $[MeSO_3H_2][Sb_2F_{11}]$ (**3**), and $[PhSO_3H_2][Sb_2F_{11}]$ (**5**) was performed on an Oxford XCalibur 3 diffractometer equipped with a Kappa CCD detector, operating with $Mo_{k\alpha}$ (0.71073 Å) radiation and a Spellman generator (voltage 50 kV, current 40 mA). The program CrysAlisPro 1.171.38.46 (Rigaku OD, 2015) was employed for data collection and reduction.[24] The structures were solved utilizing SHELXT[25] and SHELXL-2018/3[26] of the WINGX software package.[27] The structures were checked using the software PLATON.[28] The absorption correction was performed using the SCALE3 ABPSACK multi-scan method.[29] Visualization was done with the software Mercury.[30] Selected data and parameters of the measured single-crystal X-ray structure analyses are summarized in Tables S1 and S2 (see the ESI).† NMR samples were prepared by adding the HF solution to a small FEP tube under a nitrogen stream. The tube was sealed under a vacuum and inserted into a standard NMR tube. For ^{1}H, ^{13}C, and ^{19}F NMR measurements, Bruker AV400TR and JEOL ECX 400 NMR spectrometers were used. For evaluation, MNOVA by Mestrelab was used.[31] The quantum chemical calculations were performed at the B3LYP/aug-cc-pVTZ level of theory. For visualization and illustration of the MEP calculations, GaussView 6.0 was used.[32,33]

$MeSO_3H$(RT). Dried CH_3SO_3H (0.065 mL, 1.00 mmol, 1.0 eq.) was added to an FEP reactor vessel. BF_3 (68 mg, 1.00 mmol, 1.0 eq.) was condensed into the vessel together with aHF (40 mg, 2.00 mmol, 2.0 eq.) at −196 °C. The reaction mixture was warmed up to room temperature and homogenized to complete dissolution The excess solvent was removed overnight at −78 °C in a dynamic vacuum. The product was obtained as colorless crystalline solids.

$[MeSO_3H_2][AsF_6]$(RT). Dried CH_3SO_3H (0.065 mL, 1.00 mmol, 1.0 eq.) was added to an FEP reactor vessel. AsF_5 (170 mg, 1.00 mmol, 1.0 eq.) was condensed into the vessel together with aHF (40 mg, 2.00 mmol, 2.0 eq.) at −196 °C. The reaction mixture was warmed up to room temperature and homogenized to complete dissolution. The excess solvent was removed overnight at −78 °C in a dynamic vacuum. The product was obtained as colorless crystalline solids.

$[MeSO_3H_2][Sb_2F_{11}]$(RT). SbF_5 (325 mg, 1.5 mmol, 3.0 eq.) was condensed into an FEP reactor vessel together with aHF (80 mg, 2.00 mmol, 4.0 eq.) at −196 °C. Then the vessel was filled with dried CH_3SO_3H (0.033 mL, 0.50 mmol, 1.0 eq.). The reaction mixture was warmed up to room temperature and homogenized to complete dissolution. The excess solvent was removed overnight at −78 °C in a dynamic vacuum. The product was obtained as colorless crystalline solids.

$PhSO_3H$(RT). Dried $C_6H_5SO_3H$ (158 mg, 1.00 mmol, 1.0 eq.) was added to an FEP reactor vessel. BF_3 (68 mg, 1.00 mmol, 1.0 eq.) was condensed into the vessel together with aHF (40 mg, 2.00 mmol, 2.0 eq.) at −196 °C. The reaction mixture was warmed up to room temperature and homogenized to complete dissolution. The excess solvent was removed overnight at −78 °C in a dynamic vacuum. The product was obtained as a brown amorphous residue.

$[PhSO_3H_2][AsF_6]$(RT). Dried $C_6H_5SO_3H$ (158 mg, 1.00 mmol, 1.0 eq.) was added to an FEP reactor vessel. AsF_5 (170 mg, 1.00 mmol, 1.0 eq.) was condensed into the vessel together with aHF (40 mg, 2.00 mmol, 2.0 eq.) at −196 °C. The reaction mixture was warmed up to room temperature and homogenized to complete dissolution. The excess solvent was removed overnight at −78 °C in a dynamic vacuum. The product was obtained as colorless crystalline solids.

$[PhSO_3H_2][Sb_2F_{11}]$(RT). SbF_5 (1.36 g, 6.27 mmol, 10.0 eq.) was condensed into an FEP reactor vessel together with aHF (100 mg, 2.50 mmol, 4.0 eq.) at −196 °C. Then the vessel was filled with dried CH_3SO_3H (99.5 mg, 0.63 mmol, 1.0 eq.). The reaction mixture was warmed up to room temperature and homogenized to complete dissolution. The excess solvent was removed overnight at −78 °C in a dynamic vacuum. The product was obtained as colorless crystalline solids.

Conclusions

MSA and BSA react in the binary superacidic media HF/MF_5 (M = As, Sb) with the formation of sulfonium salts ($RSO_3H_2^+$). In the binary superacidic system HF/BF_3 no reaction was observed with MSA and BSA. Even providing an excess of Lewis acid, diprotonation of the sulfonic acid moiety of MSA and BSA cannot be observed at room temperature when tested up to ten equivalents. The obtained protonated salts of the monoprotonated species were isolated and characterized by low-temperature vibrational spectroscopy, NMR spectroscopy, and single-crystal structure analyses and quantum chemical data (B3LYP-aug-cc-pVTZ) were discussed. Although the link of a phenyl substituent shows larger hyperconjugative effects no disulfonium dication ($RSO_3H_3^{2+}$) could be obtained under the applied conditions. It can be estimated that full protonation of the sulfonium moiety leads to collapse of the mesomeric stabilization and therefore disulfonium dications do not exist, as it is not energetically favourable.

Conflicts of interest

There are no conflicts to declare.

Data availability

The data supporting this article have been included as part of the ESI.† Full details of vibrational spectroscopy, NMR spec-

troscopy, X-ray diffraction refinement, and computational details are provided. Crystallographic data for $MeSO_3H$ (2419553), $[MeSO_3H_2][AsF_6]$ (2419554), $[MeSO_3H_2][Sb_2F_{11}]$ (2419555), $[PhSO_3H_2][Sb_2F_{11}]$ (2419556) and $PhSO_2F{\cdot}H_2F[AsF_6]$ (2422284)† have been deposited at the CCDC and can be obtained from **https://www.ccdc.cam.ac.uk**.

Acknowledgements

Prof. Dr A. J. Kornath deceased unexpectedly in March 2024. We are grateful to the Department of Chemistry at the Ludwig Maximilian University of Munich, the Deutsche Forschungsgemeinschaft (DFG), the F-Select GmbH, and Prof. Dr Karaghiosoff for their support.

References

1 M. Naoi, W. Maruyama and K. Inaba-Hasegawa, *Curr. Top. Med. Chem.*, 2012, **12**(20), 2177–2188.
2 M. A. Sheraz, *et al.*, *J. Pharm.*, 2016, **2016**, 8961621.
3 H. G. M. Edwards, D. R. Brown, J. A. Dale and S. Plant, Raman spectroscopy of sulfonated polystyrene resins, *Vib. Spectrosc.*, 2000, **24**(2), 213–224.
4 V. Premasagar, V. A. Palaniswamy and E. J. Eisenbraun, *J. Org. Chem.*, 1981, **14**, 2974–2976.
5 D. Delcrois, B. Martín-Vaca, D. Bourissou and C. Navarro, *Macromolecules*, 2010, **43**, 8828–8835.
6 M. D. Gernon, M. Wu, T. Buszta and P. Janney, *Green Chem.*, 1999, **1**, 127–140.
7 R. Gut, *J. Fluorine Chem.*, 1980, **15**(2), 163–167.
8 R. C. Paul, V. P. Kapila, R. Kuma, S. K. Gupta and S. K. Sharma, *Z. Anorg. Allg. Chem.*, 1980, **471**, 203–207.
9 S. Brownstein and A. E. Stillman, *J. Phys. Chem.*, 1959, **63**, 2061–2062.
10 W. M. Haynes, *Handbook of Chemistry and Physics*, Taylor and Francis, Boca Raton FL, 2016, vol. 97, pp. 5–89.
11 T. Soltner, N. R. Goetz and A. J. Kornath, *Eur. J. Inorg. Chem.*, 2011, **2011**, 3076–3081.
12 V. Bockmair, A. Klöck, D. Hollenwäger and A. J. Kornath, *Acta Crystallogr., Sect. C:Struct. Chem.*, 2024, **80**, 781–786.
13 R. Seelbinder, N. Götz, J. Weber, R. Minkwitz and A. J. Kornath, *Chem. – Eur. J.*, 2010, **16**, 1026.
14 M. Hopfinger, K. Lux, F. Schubert and A. J. Kornath, *Acta Crystallogr., Sect. C:Cryst. Struct. Commun.*, 2011, **67**, 400.
15 D. V. Gerven, A. Mertens, K. Eppers, J. Nickelsen and M. S. Wickleder, *Z. Anorg. Allg. Chem.*, 2024, **650**, e202400019.
16 F. H. Allen, O. Kennard and D. G. Watson, *J. Chem. Soc.*, 1987, **2**, 1–19.
17 P. Manana, E. C. Hosten and R. Betz, *Z. Kristallogr. - New Cryst. Struct.*, 2021, **36**(1), 97–99.
18 K. Bartmann and D. Mootz, *Acta Crystallogr., Sect. C:Cryst. Struct. Commun.*, 1990, **46**, 319–320.
19 L. Zhong and S. F. Parker, *R. Soc. Open Sci.*, 2018, **5**, 181363.
20 M. Hopfinger, K. Lux and A. Kornath, *ChemPlusChem*, 2012, **77**, 476.
21 M. Hopfinger, F. Zischka, M. Seifert and A. Kornath, *Z. Anorg. Allg. Chem.*, 2018, **644**, 574–579.
22 D. Leitz, M. Hopfinger, K. Stierstorfer, Y. Morgenstern, J. Axhausen and A. Kornath, *Z. Anorg. Allg. Chem.*, 2017, **643**, 1202–1207.
23 L. Bayersdorfer, R. Minkwitz and J. Jander, *Z. Anorg. Allg. Chem.*, 1972, **392**(2), 137–142.
24 Rigaku Oxford Diffraction, *CrysAlisPro Software System; Version 1.171.39.46e*, 2018.
25 G. M. Sheldrick, SHELXT - integrated space-group and crystal structure determination, *Acta Crystallogr., Sect. C: Struct. Chem.*, 2015, **71**(1), 3–8.
26 G. M. Sheldrick, Crystal structure refinement with SHELXL, *Acta Crystallogr., Sect. C:Struct. Chem.*, 2015, **71**(1), 3–8.
27 L. J. Farrugia, WinGX suite for small-molecule single-crystal crystallography, *J. Appl. Crystallogr.*, 1999, **32**(4), 837–838.
28 A. L. Spek, Single-crystal structure validation with the program PLATON, *J. Appl. Crystallogr.*, 2003, **36**(1), 7–13.
29 *SCALE3 ABSPACK, an Oxford Diffraction Program*, Oxford Diffraction Ltd, 2005.
30 C. F. Macrae, I. Sovago, S. J. Cottrell, P. T. A. Galek, P. McCabe, E. Pidcock, M. Platings, G. P. Shields, J. S. Stevens, M. Towler and P. A. Wood, Mercury 4.0: from visualization to analysis, design and prediction, *J. Appl. Crystallogr.*, 2020, **53**(1), 226–235.
31 *Mestrelab Research S. L. MestReNova. Version 14.0.0*, 2019.
32 M. J. Frisch, G. W. Trucks, H. B. Schlegel, G. E. Scuseria, M. A. Robb, J. R. Cheeseman, G. Scalmani, V. Barone, B. Mennucci, G. A. Petersson, H. Nakatsuji, M. Caricato, X. Li, H. P. Hratchian, A. F. Izmaylov, J. Bloino, G. Zheng, J. L. Sonnenberg, M. Hada, M. Ehara, K. Toyota, R. Fukuda, J. Hasegawa, M. Ishida, T. Nakajima, Y. Honda, O. Kitao, H. Nakai, T. Vreven, J. A. Montgomery, J. E. Peralta, F. Ogliaro, M. Bearpark, J. J. Heyd, E. Brothers, K. N. Kudin, V. N. Staroverov, R. Kobayashi, J. Normand, K. Raghavachari, A. Rendell, J. C. Burant, S. S. Iyengar, J. Tomasi, M. Cossi, N. Rega, J. M. Millam, M. Klene, J. E. Klene, J. E. Know, J. B. Cross, V. Bakken, C. Adamo, J. Jaramillo, R. Gomperts, R. E. Stratmann, O. Yazyev, A. J. Austin, R. Cammi, C. Pomelli, J. O. Ochterski, R. L. Martin, K. Morokuma, V. G. Zakrzweski, G. A. Voth, P. Salvador, J. J. Dannenberg, S. Dapprich, A. D. Daniels, O. Farkas, J. B. Foresman, J. V. Ortiz, J. Cioslowski and D. J. Fox, *Gaussian 16*, Revision C.01, Gaussian Inc., Wallingford CT, 2016.
33 *Rev. C.01; Gaussian, 2016. (36)*; D. Roy, A. Keith Todd and J. M. Millam, *GaussView. Version 6*, 2019.